How to improve x-ray scattering techniques to quantify bone mineral density using spectroscopy

M. Krmar
Department of Physics, California State University Dominguez Hills, Carson, California 90747 and Department of Physics, University of Novi Sad, Novi Sad, Serbia

K. Ganezer[a)]
Department of Physics, California State University Dominguez Hills, Carson, California 90747

(Received 13 September 2011; revised 2 February 2012; accepted for publication 2 February 2012; published 14 March 2012)

Purpose: The purpose of this study was to develop a new diagnostic technique for measuring bone mineral density (BMD) for the assessment of osteoporosis, which improves upon the coherent to Compton scattering ratio (CCSR) method, which was first developed in the 1980s. To help the authors achieve these goals, they have identified and studied two new indices for CCSR, the forward scattered to backward scattered (FS-BS) and the forward scattered to transmitted (FS-T) ratios. They believe that, at small angles, these two parameters can offer a practical *in vivo* determination of BMD that can be used to overcome the limitations of past CCSR systems, including high radiation dosages, costs, and examination durations.

Methods: In previous CCSR studies, a high-activity radioactive source with a long half-live (usually ^{241}Am) and an expensive and bulky cryogenic HPGe detector were applied to both *in vivo* and *in vitro* measurements. To make this technique more suitable for clinical applications, the possibility of using a standard diagnostic x-ray tube generating a continuous spectrum was investigated in this paper. Scattered radiation from trabecular bone-simulating phantoms containing various mineral densities that span the normal range of *in vivo* BMD was collected in this study using relatively inexpensive noncryogenic CdTe or NaI detectors.

Results: The initial results demonstrate that a modified version of CCSR can be successfully applied to trabecular bone assessment using a diagnostic x-ray tube with a continuous spectrum in two variations, the FS-BS and the FS-T ratio. When FS-BS is measured, intensity spectra in the forward and backward directions must be collected while FS-T requires only the integral intensity of the scattered and transmitted (T) spectra in the energy region above 40 keV. For both of these methods, forward scattering angles less than or equal to 15° and backward scattering angles greater than or equal to (165°= 180° − 15°) are needed.

Conclusions: The authors determined that FS-T is more sensitive to changes in BMD than transmission or absorption alone and that the FS-BS method can yield an absolute measurement of the mean atomic number of the scattering medium, after a correction for path-dependent attenuation. Since this study determined that the FS-T ratio is independent of the incident energy over a broad energy region, it will be possible to apply FS-T to bone densitometry using inexpensive integral photon detectors. The authors believe that, by replacing the radionuclide source with an x-ray tube and the cryogenically cooled HPGe detector with a single solid state CdTe, NaI, or silicon detector or an annular array of detectors, as suggested in this study, the past difficulties of CCSR concerning high radiation exposure, costs, and durations as well as lack of convenience can be overcome and that CCSR could eventually become popular in clinical settings. © *2012 American Association of Physicists in Medicine*. [http://dx.doi.org/10.1118/1.3687162]

Key words: x-ray scattering and spectroscopy, bone assessment

I. INTRODUCTION

The CCSR method was first described by Puumalainen *et al.*[1] who formulated a diagnostic method for the determination of trabecular bone mineral density (TBD), based upon the simultaneous measurement of two components of gamma radiation that were scattered in a selected volume of trabecular bone.[1] In these and other early studies, it was determined theoretically and verified experimentally that the intensity ratio of coherent to Compton scattered beams (CCSR) was strongly dependent upon the effective (or mean) atomic number of the scattering material,[2–6] Z_{eff}. In particular, the theoretical proportionality between CCSR (R), the atomic number (Z), and the magnitude of the momentum transfer (x) is governed by the ratio of form factors $[F(x, Z]^2/S(x, Z)$, where $F(x, Z)$ is the atomic form factor and $S(x, Z)$ is the incoherent scattering function. For both trabecular bone and soft tissue, Ref. 1 shows that the form factors yield a simple power law proportionality

between R (CCSR) and Z given by $R \sim Z^b$, where b was estimated to be approximately equal to 3 for a wide range of values of Z that vary from 7.5 to 100, experimentally[1] as well as theoretically.[1,4] Therefore, the sensitivity of CCSR for bone studies is quite high ($b = 3$ in the power law) compared to the likelihood for simple absorption or for Compton scattering,[7] which are proportional to only the first power of Z ($b = 1$).

The rate of turnover for trabecular bone is about eight times higher than that of solid bone, a relationship that implies that TBD can be a very sensitive index for the diagnosis and monitoring of metabolic bone diseases such as osteoporosis. The principal advantage of CCSR and other conceivable scattering techniques over transmission methods for bone diagnostics including dual energy methods are their ability (along with QCT) to isolate trabecular bone and to measure volumetric rather than areal density where the volume of interest (VOI) in trabecular bone is defined by the intersection of the collimated gamma ray beam and the projection of the detector collimator. Another advantage of CCSR is the fact that the attenuation on surrounding tissues is almost the same for both the coherent and Compton components.

To isolate the coherent and Compton peaks in spectra from scattered x-rays without significant overlap among the two peaks, it is necessary to use radioactive sources having one or two well separated and intense gamma lines, even when high resolution HPGe detectors are available. This constraint limits the choice of energy to only a few suitable heavy isotopes. The origin of the incident gamma radiation in early CCSR studies was a radionuclide, ^{241}Am, source with a high activity of a few giga-becquerels and a long half-life of 432 years that requires strict radiation safety measures. Scattered beams were measured at a variety of angles,[8–10] from 22.5° to 135°, and CCSR was tested using K_2HPO_4 water solutions[2,4,11] on phantoms made from trabecular bone ash and petrolatum[5,12] and on human subjects[13,14] where trabecular bone in the calcaneous (the heel) served as the scattering material. Most previous CCSR studies obtained good energy resolution and sensitivity through the use of large scattering angles (around 90°). One study determined that the sensitivity, obtained from the slope of a linear fit to data on CCSR as a function of atomic number (Z), increases uniformly with scattering angle between 30.2° and 93.6°.[3] For small angles, the coherent component is the dominant source of radiation. For example, at an energy of 60 keV, an atomic number of $Z = 12$, and a forward scattered of $\theta = 10°$, the coherent scattering cross-section is more than six times higher than that of Compton scattering. For atomic numbers from 7 to 12 and for a scattering angle of $\theta = 10°$, the intensity of the coherent component increases by a factor of about seven, while the increase from $Z = 7$ to $Z = 12$ is only about 25% for the Compton intensity. However, the best justification for the use of small-angle scattering in a new CCSR system is based upon the observation that the intensity of scattered coherent radiation at small angles is a couple of orders of magnitude higher than that at high angles. For example, in a $Z = 10$ material, the cross-section for coherent scattering for 60 keV photons at 10° is 270 times higher than that for coherent scattering at 90° for the same energy. Therefore, we believe that the usage of small-angle coherently scattered photons in a new *in vivo* CCSR system offers the promise of significantly reducing radiation exposure.

This study focused on the feasibility of applying a standard x-ray tube to the CCSR technique and on developing an x-ray scattering method, which uses small-angle scattering for bone densitometry as opposed to the large angles of approximately 70°, which were used in traditional CCSR. Since a spectrum from an x-ray tube is continuous, an energy region in which the coherent and the Compton scattered components overlap is unavoidable. Therefore, we searched for quantities that were sensitive functions of bone mineral density (BMD) referred to as indices that were related to the forward scattered (FS), backscattered (BS), and transmitted (T) intensities, which are easily defined and separated by the different scattering angle (θ) assigned to each of these components. We also formulated simple methods for using the indices to determine BMD. The search for indices was complicated by the fact that that the FS-BS and FS-T intensities that are easily measured in scattering experiments are usually a mixture of both coherent and Compton photons, which cannot be distinguished from each other on a photon-by-photon basis but are observable on a statistical basis because increases in the proportion of coherently scattered photons, especially at small angles, show up as excesses in the total number of scattered photons in the FS, BS, and T intensities and excesses in the FS-BS and FS-T ratios.

Other major goals of this study were to characterize the dependence of $R(FS/BS)$ and $R(FS/T)$ on the mineral concentration of test objects that simulate trabecular bone and to characterize the energy dependence of $R(FS/BS)$ and $R(FS/T)$. To achieve these goals, we collected complete spectra from a diagnostic x-ray tube of FS, BS, and T beams after interacting with test objects, using energy sensitive solid state detectors, and characterized the variation of $R(FS/BS)$ and $R(FS/T)$ as a function of BMD for several different energy regions. We determined that if these measurements were repeated and averaged over several pairs of (complementary) FS and BS angles, the effects of variable attenuation along the different paths of the FS, BS, and T beams could be eliminated.

This study was also motivated by the bone assessment literature, which suggests that, even though several different radiological methods are currently or were formally used in bone diagnostics, as outlined in Table I, which displays performance parameters of current bone densitometry methods with those of CCSR in the past and possibly in the future (as outlined in Sec. IV), a need for new and improved techniques such as the authors' scattering methods persists. For example, QCT scanners are relatively expensive and are constantly in use for procedures that are more urgent than routine bone assessment. In addition, Table I indicates that QCT for bone density measurements[15] has a high dosage of 50 μSv or more[16,17] and is relatively imprecise with systematic errors that are about 7% or higher because of its reliance on multiple spectra from different thin slices. It is notable that the scattering methods described in this study when used

TABLE I. Accuracy, precision, and dosage of various present modalities for bone assessment and the CCSR methods used in the past.

Modality	Precision uncertainty	Accuracy uncertainty	Radiation exposure (μSv)
Radiographic absorptiometry phalanx or metacarpal	1–2% 1–2%	5%	~5 50
SXA radius or calcaneous	1–2% 1–3% *<1–2%*	4–6%	≤1 *<10*
QCT in whole spine	2–4%, 2–4%, 1–5%	4–8%, 4–5%	≤50 500
DXA			
PA spine	1–1.5% 1–2%	4–10%	~1 10–50
Radius or calcaneous	1–2% 1–3%	4–6%	≤1 10
Proximal femur	1.5–3%	6%	~1
Whole body	~1%	3%	~3
CCSR of the past (Ref. 18)	3%	5%	3000
Possible values of the authors' CCSR-related methods in the future	Not available[a]	1.5–3.7%	≤5000[b], 50[c]

Entries in this table are from Cummings *et al*. (Ref. 16) (in bold font), Greenfield (Ref. 18) (plain font), Tothill (Ref. 19) (Italicized), Karellas *et al*. (Ref. 3) (for past CCSR, plain font), Genant *et al*. (Ref. 17) (underlined font), this study (for future CCSR, plain font). To convert from rems to Sieverts (Sv), note that 1 rem = 0.01 Sv = 10 mSv and 1 mrem = 10 μSv.

[a]The precision uncertainty of the authors' CCSR-related methods will be undertaken in follow-up studies, since currently, only a small fraction of this error due to count rates statistics can be calculated.

[b]This value of 5000 μSv is for the system used to make the measurements in this paper with a small CdTe detector and should be taken to be an upper limit on the dosage.

[c]With the usage of a much larger ring-shaped detector and other methods to decrease dosage such as the usage of broader energy intervals, the authors will very likely be able to lower the dosage to a value of 50 μSv, which might be considered to be a lower limit on the dosage.

with a ring detector might be able to achieve a comparable dosage to the 50 μSv of QCT, which could be as low as 50 μSv and thus within a factor of 50 of DXA and much closer in some estimates and cases (Table I). DXA has a relatively high accuracy of 3–10%, a high precision of approximately 1–3%,[16,17] a low dosage of a few micro-Sieverts and a lower device cost than QCT of about $70K–$100K. The authors' scattering methods measure the volumetric density, which is an important index in certain relatively common cases, such as those in which the region of interest has a large thickness, when BMD is quickly changing as in pediatrics, the early stages of paraplegia, or bone lose in females due to low body weight or fat levels, as in amenorrhea, in regions with high proportions of both trabecular and cortical bone and in other cases when a two-dimensional projection is not a good approximation.

Small-angle scattering techniques can isolate a specific volume inside a selected region of trabecular bone, therefore providing a great advantage over DXA, which does not provide a clear distinction between the three major components in bone densitometry: trabecular bone, cortical bone, and soft tissue. Although QCT can also distinguish between these three components and can also provide information on density (in terms of BMD) as well as a clearly defined position for each density measurement, it has the best chance of accurately predicting bone strength of all of bone diagnostic modalities. However, the FS-T method presented here requires only a simple system, which would likely be available at a significantly lower cost than QCT. Small-angle scattering methods can also yield the mean value of the atomic number and subsequently the volumetric density of a specific region in the body.[20–22] The possible errors due to patient repositioning in the authors' scattering methods are likely comparable to those found in beam placement in image guided radiation therapy, of the order of a few millimeters, such as the 2–3 mm found in Ref. 23 for setup errors in external beam radiation therapy using electronic portal imaging. In cases in which the selected volume is sufficiently small and at a large distance from the cortical envelope, accurate positioning is not crucial since the authors' irradiated volume will still be inside the region that contains trabecular bone, even if positioning is imperfect. Once a correction for varying amounts of attenuation in different paths, as described below in Sec. III C, is completed, the volumetric density obtained using our scattering methods has the advantage of being nearly free from beam hardening (the loss of low energy photons),[20,24] as well as other sources of uncertainties caused by variable attenuation properties in different paths or tissues including those associated with the uncertainty in the fat distribution.

II. MATERIALS AND METHODS

II.A. Theory

II.A.1. The forward scattered–backscattered ratio

II.A.1.a. Monoenergetic radiation (from a gamma ray source). We assume that gamma ray photons from a narrow beam are scattered by an object (of atomic number Z), at an angle relative to the beam direction of θ as established by the collimators, and are collected using an HPGe detector. In this case, the spectrum will contain two distinct maxima: the first being the narrow, coherent peak, which has the same energy as that of the incident radiation (E), while the second maximum is the broader Compton peak, at a slightly lower energy. The width of the coherent peak is comparable to the spectroscopic width of gamma lines of the same energy, while the width of the Compton peak depends upon the degree of collimation. The ratio of the coherent to Compton scattered intensities is given by the following relationship:

$$CCSR = \frac{I_{coh}(E,Z,\theta)}{I_{Com}(E',Z,\theta)} = \frac{d\sigma_T/d\Omega}{d\sigma_{K-N}/d\Omega}\frac{[F(x,Z)]^2}{S(x,Z)}, \quad (1)$$

where $d\sigma_T/d\Omega$ represents the well known Thomson differential scattering cross-section per electron, $F(x, Z)$ is the atomic form factor, and x is the momentum transfer variable, a quantity that is dependent on both the photon energy and the scattering angle,[4] $d\sigma_{K-N}/d\Omega$ is the Klein–Nishina (differential) cross-section for free electrons, and $S(x, Z)$ is the incoherent scattering function. The values of the form factor $F(x, Z)$ and the incoherent scattering function $S(x, Z)$ as a function of x and Z are available in the standard reference tables.[14] For the selected photon energy (E) and scattering angle (θ), CCSR is a function of the mean atomic number of the scattering medium (Z). Therefore E, θ, and Z are the major parameters that are studied and varied in this paper. The composition of trabecular bone includes trabeculai, fatty tissue, collagen, and other components, and the mean Z for of the VOI can uniquely determine BMD. Therefore, Z and BMD are taken to be equal in the rest of this paper.

In this study, we found an explicit expression for sensitivity as a function of scattering angle as follows. Theoretical predictions for CCSR were calculated using Eq. (1) for $Z=7$ and $Z=12$, the approximate atomic numbers of soft tissue and bone, respectively, for several values of θ between 2° and 112°. It is widely accepted that the average value of Z for trabecular bone is between 7 and 12.[4] The ratio of CCSR for $Z=12$ divided by that for $Z=7$, $\mathrm{CCSR}_{(Z=12)}/\mathrm{CCSR}_{(Z=7)}$, was used as an index of the sensitivity of CCSR to Z for the scattering material. Calculations were performed for several different energies between 40 and 100 keV. The results of these computations are given in Fig. 1, which assumes that the incident energy is 60 keV. It is evident from Fig. 1 that the $\mathrm{CCSR}_{(Z=12)}/\mathrm{CCSR}_{(Z=7)}$ ratio increases uniformly for all values of θ in excess of 30°, although there is a region with a peak in the sensitivity at small angles. The maximum value of $\mathrm{CCSR}_{(Z=12)}/\mathrm{CCSR}_{(Z=7)}$ (the sensitivity index) was almost the same for all energies considered in the authors' calculations, because relative changes of products of the coherent and Compton cross-sections and appropriate parameters $F(x, Z)$ and $S(x, Z)$ for different atomic numbers at the same energy nearly cancel each other out.[25,26] The value of θ at maximum sensitivity was calculated as a function of energy. We found that the scattering angles of maximum sensitivity for 40, 60, and 100 keV are approximately 18°, approximately 12°, and slightly less than 8°, respectively.

The data in Fig. 1 demonstrate that, for all angles greater than 60°, the sensitivity is higher than that of the peak at small angles. However, there is one very significant advantage associated with the usage of small scattering angles: Coherent scattering dominates at small angles where the fraction of coherently scattered photons exceeds 50%, and this fraction increases with Z. For example, at 60 keV and $Z=12$, the differential coherent scattering cross-section is more than five times higher than the differential cross-section for Compton scattering at 10°. In the range of atomic numbers between 7 and 12, the intensity of the coherent component increases by a factor of about seven while the increase for the Compton intensity from $Z=7$ to $Z=12$ is only about 25%. However, the best justification for the use of low-angle scattering for a new scattering or CCSR system

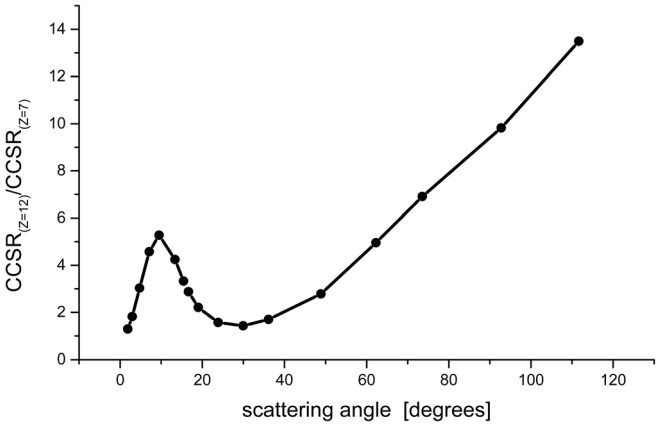

FIG. 1. The ratio of $\mathrm{CCSR}_{(Z=12)}/\mathrm{CCSR}_{(Z=7)}$ as a function of scattering angle at an incident energy of 60 keV. Tabular values (Ref. 26) for the form factor $F(x, Z)$ were used in this simulation.

is likely based upon the fact that the intensity of coherent scattered radiation at low angles is a couple of orders of magnitude higher than that at high angles. For example, in a $Z=10$ material, the cross-section for coherent scattering of 60 keV photons at 10° is 270 times higher than that for coherent scattering at 90° at the same energy. Therefore, the usage of low-angle coherently scattered photons for *in vivo* bone densitometry offers the promise of significantly reducing radiation dosage.

For an incident x-ray energy of 60 keV, the energy differences between coherent and Compton scattered photons for $\theta=10°$, $\theta=12°$, and $\theta=15°$ are 0.11, 0.15, and 0.24 keV, respectively. These small differences are less than the resolution of an HPGe detector; thus, there is no way to distinguish the coherent and Compton components from the photons contained in the single peak in the spectrum of scattered x-rays. In this case, the total intensity is given by the following simple formula:

$$I_{tot}(E, Z, \theta) = I_0 N A \varepsilon(E) \left(\frac{d\sigma_{coh}}{d\Omega} + \frac{d\sigma_{Com}}{d\Omega} \right), \quad (2)$$

where I_0 is the intensity of the incident radiation, N is the areal density of atoms in the irradiated object, A is a factor describing the total attenuation of the beam in the object before and after coherent scattering, and $\varepsilon(E)$ is the absolute efficiency of the detection system at the detected x-ray energy (E). The availability of two well separated peaks in the spectrum of scattered x-rays at large angles allows for an easy and accurate calculation of CCSR as the ratio of the intensities of the coherent and Compton scattered photons (CCSR). In this case, all quantities except for the differential cross-sections cancel out when CCSR is calculated (from the spectrum), and the results are independent of the effects of attenuation in surrounding tissues, as well as the detector characteristics such as efficiency. However, the summed intensity of the nonresolved peaks [in Eq. (2)], although a strong function of Z, is also dependent upon the geometry of the measurement setup, the attenuation properties of the scattering medium and the surrounding tissues, and the physical properties of the detector such as efficiency and response.

An example of a feasible and promising geometrical configuration for x-ray scattering is outlined in Fig. 2(a). The intensity of the FS radiation at an angle θ can be normalized by the intensity of the BS radiation detected at a (complementary) angle of $(180^\circ - \theta)$, since the volume of the scattering medium in both cases is nearly the same. A small difference may remain due to divergences in the collimator openings in front of the detector, although this effect can be minimized by using narrow collimation. The use of simultaneous measurements for both the FS and BS spectra can also minimize the dependence of the intensity ratio upon the input intensity I_0.

When the energy of the incident beam is 60 keV and the FS and BS scattering angles are 15° and 165°, the energy difference between the forward and backward scattered components is about 11 keV. Different penetration abilities and possible differences in the thicknesses of the surrounding tissues can result in varying amounts of attenuation among the FS and BS beams. If one makes the assumption that the attenuation in the forward and backward directions is equal, as in Secs. II A 1 b and II A 1 c below, analyses of CCSR involving FS and BS intensities can be significantly simplified.

If the radiation source is a radioisotope with a single intense gamma line such as ^{241}Am, as is commonly used in CCSR, the backscattered Compton component will be well separated from the coherent component. In this case, it is possible to determine the intensity of the backscattered Compton radiation and to calculate FS-BS from the following expression:

$$R(FS/BS) = \frac{I_{FS}(Z,\theta)}{I_{BS}(Z,180+\theta)} = \frac{(I_{coh}(Z,\theta)+I_{Com}(Z,\theta))_{FS}}{(I_{Com}(Z,180+\theta))_{BS}} = k\left(\frac{\frac{d\sigma_{coh}(Z,\theta)}{d\Omega}+\frac{d\sigma_{Com}(Z,\theta)}{d\Omega}}{\frac{d\sigma_{Com}(Z,190+\theta)}{d\Omega}}\right), \quad (3)$$

where the variable k contains the ratio of all noncanceling parameters related to the scattering volume, the attenuation characteristics of the volume, and the detector efficiencies for the FS and BS beams.

II.A.1.b. Use of an x-ray tube as a source of radiation. The performance of a CCSR device can be enhanced by replacing the radionuclide line source with an x-ray tube that generates a continuous spectrum. In the forward direction, for any convenient energy window, both the FS and BS components of the scattered radiation will be present with nearly identical energies, as in the case of a monoenergetic gamma ray source. It is noteworthy that the backscattered beam will contain x-rays whose incident energy of 60 keV has been Compton shifted to lower energies combined with 48.6 keV photons that result from the coherent scattering of primary beam photons at an angle of 170°. An important consideration is the dependence of the Compton shift upon the incident energy. For example, at 80 keV, photons that are Compton scattered at 170° will decrease in energy by 19 keV. The strong tendency of coherent radiation to decrease in intensity with increasing scattering angle greatly simplifies detection of the backscattered photons. For a scattering material with $Z = 7$, at an incident energy 60 keV, and angles of about $\theta = 170^\circ$, the intensity of the coherent component is only about 0.5% of that of the Compton component. For the same incident energies, backward scattering angles, and an atomic number (in the scattering volume) of $Z = 12$, the coherent radiation has a slightly higher intensity than that of the Compton component by a factor of about 0.8%. This result implies that the intensity of coherently scattered photons at high angles near $\theta = 180^\circ$ can be neglected, which results in a considerable simplification of the data analysis. For a continuous spectrum generated by an x-ray tube, some portion of the spectrum (called an energy window) emitted in the forward direction can be used to determine the total intensity (within the chosen window). The corresponding window for of the backscattered spectrum can be determined by correcting the energy limits of the FS window by the Compton shift. The spectrum of the backscattered radiation can be assumed to consist entirely of Compton radiation and the FS-BS ratio can be calculated using Eq. (3).

The use of a radionuclide source in CCSR measurements has one major limitation: Only a small number of discretely spaced energies (often only one or two lines) are emitted by the source and are, therefore, available for scattering. A significant advantage is offered by the use of a spectrum from an x-ray tube because the tube yields a continuous range of energies from the threshold energy to the maximum energy determined by the peak value of the accelerating potential.

II.A.1.c. The attenuation correction. Attenuation poses a serious problem for the quantitative determination of BMD using scattered radiation. In standard CCSR, both coherent and Compton photons travel through identical pathways to a single detector. However, a more complex issue is the fact that the Compton component has a lower energy than that of the coherent component and that the attenuation coefficient varies with energy, although this affect has yet to be described in detail in the literature.

For the FS-BS configuration, each transmitted or scattered beam has a different source-target-detector path. In *in vivo* applications, the geometry of the trabecular and cortical bone is often nonuniform and irregular, with bone dimensions varying from patient to patient. In addition, the energy of backward scattering is lower than that of forward scattering. Therefore, each beam may yield a measured attenuation that deviates significantly from its real value. Corrections for the resulting errors can be made using a simple rotational mechanism and by making corresponding modifications for anomalies in the test object or irradiated region of the body. Figure 2(a) depicts steel collimators that create shielded channels for incident and scattered x-ray beams interacting with a region of interest (ROI) inside the body comprising bone, fat, and soft tissue. It is assumed that the ROI is situated inside a volume containing only trabecular bone. The FS radiation has an almost identical energy (E_0) to that of the incident beam (IB) and the transmitted beam (T) while the lower energy of the BS radiation is denoted by E_B. If it is assumed that the detection efficiency function $\varepsilon(E)$ and the areal density N are the same for both the FS and BS beams, the factor k in Eq. (6) simplifies to the ratio of the

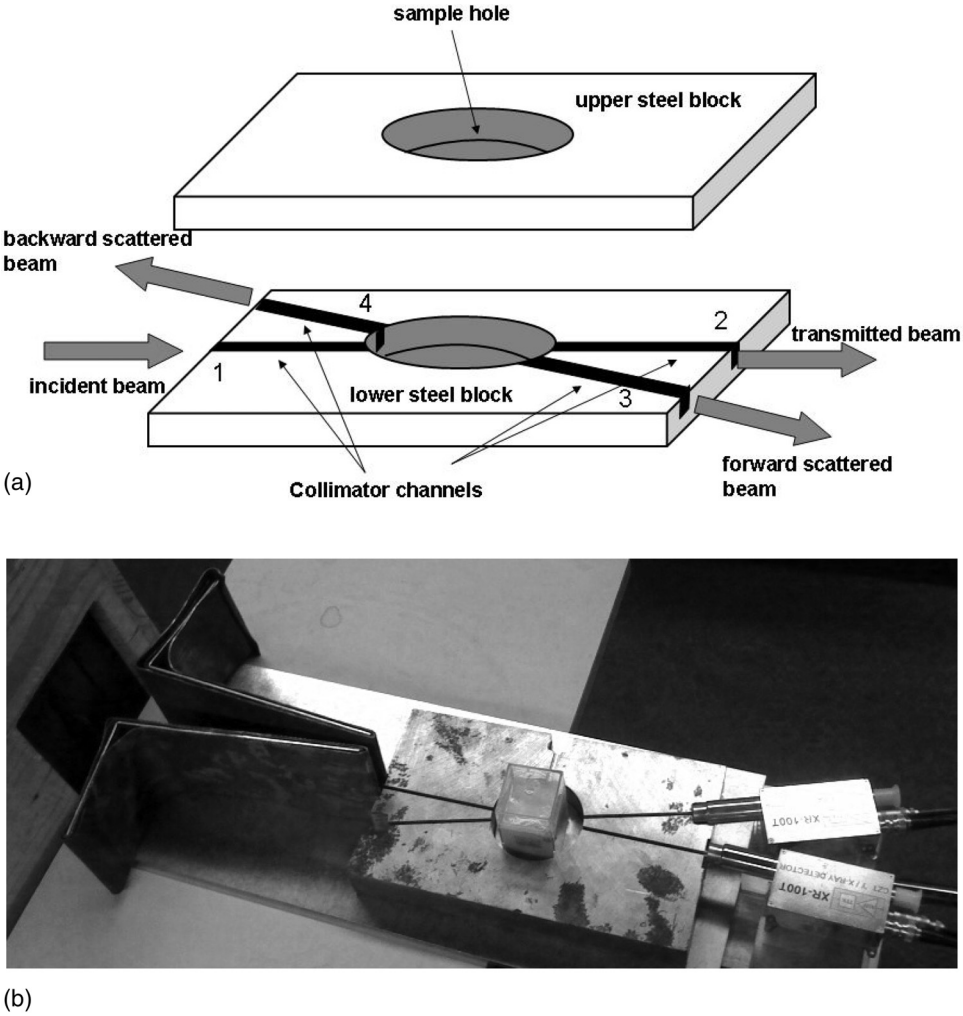

FIG. 2. (a) A schematic of the experimental setup used for the FS–BS studies performed in this study. Included are collimators made from steel blocks, narrow shielded channels called beam-lines at forward angles of 10°, 15°, and 20°, at (complimentary) backward angles equal to 170°, 165°, and 160°, and at 90° and 180°, and 6 cm diameter central holes for samples including bone phantoms. Channels were about 20 cm long on either side of the sample hole. Widths were 1, 2, and 3 mm for the 10°, 15°, and 20° forward scattered, and for the 170°, 165°, and 160° backward scattered channels. (b) A photograph showing the FS–T configuration with the x-ray tube inside a shielded box, collimator channels for $\theta = 20°$ FS and T beams with the upper plate removed in order to show the beam channels, and two CdTe detectors to collect the FS and T radiation, and phantom #10 in the sample hole. A detector can be placed at the opposite end of the channel containing the FS beam to collect the BS beam.

transmission factors of the coherent and Compton beams as they propagate along specified paths through the irradiated body. If an object having a heterogeneous structure is irradiated by an x-ray beam traveling in a single direction, at an angle of $\theta = 0°$ (for example) as illustrated in Fig. 2(a), and the coherently scattered radiation travels along paths 1 and 3 while the Compton radiation travels through paths 1 and 4 [as in Fig. 2(a)], the factor k will be given by the following equation:

$$k(0°) = \frac{\exp\left(-\sum \mu_i(E_0)x_i\right)_1 \cdot \exp\left(-\sum \mu_i(E_0)x_i\right)_3}{\exp\left(-\sum \mu_i(E_0)x_i\right)_1 \cdot \exp\left(-\sum \mu_i(E_B)x_i\right)_4}, \quad (4)$$

where μ_i and x_i are the attenuation coefficients and the thicknesses of the materials in the paths denoted by subscripts 1, 2, 3, and 4, respectively. The following similar expression for k is obtained when the ROI is irradiated from the opposite direction $180° - \theta$ (i.e., irradiation at 180° for an initial angle of $\theta = 0°$):

$$k(180°) = \frac{\exp\left(-\sum \mu_i(E_0)x_i\right)_2 \cdot \exp\left(-\sum \mu_i(E_0)x_i\right)_4}{\exp\left(-\sum \mu_i(E_0)x_i\right)_2 \cdot \exp\left(-\sum \mu_i(E_B)x_i\right)_3}. \quad (5)$$

In this case, the product of the two forward scattered to backward scattered ratios, $R(FS/BS)^{(0°)}$ and $R(FS/BS)^{(180°)}$ is given by the following equation:

$$R(FS/BS)^{(0°)} \cdot R(FS/BS)^{(180°)} = R^2 \cdot \frac{\exp\left(-\sum \mu_i(E_0)x_i\right)_3 \cdot \exp\left(-\sum \mu_i(E_0)x_i\right)_4}{\exp\left(-\sum \mu_i(E_B)x_i\right)_3 \cdot \exp\left(-\sum \mu_i(E_B)x_i\right)_4}. \quad (6)$$

This expression can be simplified to a more compact form as follows:

$$R(FS/BS)^{(0°)} \cdot R(FS/BS)^{(180°)} = R^2 \cdot \frac{I_R(E_0(3-4))}{I_R(E_B(3-4))}. \quad (7)$$

The term $I_R(E_0(3\text{-}4))/I_R(E_B(3\text{-}4))$ in Eq. (7) is simply the ratio of the relative changes of intensities (due to attenuation)

in two energy regions of an x-ray spectrum transmitted through an object along the path denoted by (3-4). Therefore, a single direct spectrum of an x-ray beam transmitted through the (3−4) path, as well as two additional spectra at 0° and 180° are first recorded and analyzed and three measurements are required to complete a single cycle of the attenuation correction procedure. For the case of the 0° and 180° measurements, the full spectrum for each of the scattered and transmitted beams should be collected. Transmitted data are needed only in step-3, which involves the (3-4) path in the attenuation correction, in order to allow for the calculation of the unknown attenuation factor; therefore, a low (incident) x-ray intensity can be used in step-3 to minimize radiation dosage.

II.A.2. The forward scattered–transmitted ratio. The intensity of small angle forward scattering, properly normalized, can be used to determine BMD. For small scattering angles, such as $\theta = 15°$, transmitted and scattered photons follow similar paths and undergo a similar amount of attenuation. Some of the parameters associated with the experimental setup such as the detector efficiency function $\varepsilon(E)$ and the intensity of the incident radiation (I_0) are canceled when the FS-T ratio is taken. For small θ, the ratio of the forward scattered intensity to the transmitted intensity ($R_{FS/T}$) is proportional to the sum of the coherent and Compton components as follows:

$$R_{FS/T} = \frac{I_{FS}(Z,\theta)}{I_T(Z,\theta)} = k' \cdot a' \cdot \left(\frac{d\sigma_{coh}(Z,\theta)}{d\Omega} + \frac{d\sigma_{Com}(Z,\theta)}{d\Omega}\right) k' \cdot a' \cdot N(Z,\theta). \quad (8)$$

The small differences between the irradiated volumes and attenuation coefficients for the forward scattered and transmitted beams are described by the parameters k' and a', respectively. The (differential cross-section) function $N(Z,\theta)$ depends upon Z and θ for a fixed incident energy E. As in the case of the FS-BS ratio ($R_{FS/BS}$), data on cross-sections from the standard tables[26] can be used to determine the theoretical values for the FS-T ratio ($R_{FS/T}$), and the sensitivity of $R_{FS/T}$ increases with decreasing values of θ and E.

For cases in which the parameters k' and a' are accurately estimated or can be neglected due to the use of similar paths for the forward scattered and the transmitted beams, $R_{FS/T}$ can be used as an absolute measure of Z for the scattering medium. When the possible influences of different attenuation paths are estimated using the procedure described in Sec. II A 1 c above, we obtain the following equation for the product of the FS-T ratios at 0° and 180°:

$$R(FS/T)^{(0°)} \cdot R(FS/T)^{(180°)} = N(Z,\theta)^2 \cdot \frac{\exp\left(-\sum \mu_i(E_0)x_i\right)_3 \cdot \exp\left(-\sum \mu_i(E_0)x_i\right)_4}{\exp\left(-\sum \mu_i(E_B)x_i\right)_1 \cdot \exp\left(-\sum \mu_i(E_0)x_i\right)_2}. \quad (9)$$

The expression in Eq. (9) can be simplified to the following compact form:

$$R(FS/T)^{(0°)} \cdot R(FS/T)^{(180°)} = N(Z,\theta)^2 \cdot \frac{I_R(E_0(3-4))}{I_R(E_0(1-2))}. \quad (10)$$

As in the case of the FS-BS method, the attenuation correction is a relative transmission factor for photons of energy E_0 in the (3-4) path relative to that of the (1-2) path that can be determined with three initial measurements that are analogous to those made in the FS-BS attenuation correction. It is notable that a simple distance correction without rotational corrections would be sufficient in the case of FS-T if two components of the same energy travel through very similar paths and distances that are distinguished only by a small change in the scattering angle ($\Delta\theta$).

The three measured intensities in this study were computed from the following:

1. The FS beam from photons scattered at small angles of up to 15° that are mostly the products of coherent scattering. Since the coherent intensity depends on the third power of the mean atomic number of the scattering medium, increased numbers of coherent photons significantly improve sensitivity to BMD;
2. The BS beam is composed of photons that are scattered at high angles close to 180° that are the products of Compton scattering with a negligible amount of coherently scattered photons. The BS intensity is subsequently used to normalize the FS component in the calculation of the FS-BS ratio; and
3. The T beam, whose intensity is used to normalize the FS component in the FS-T ratio.

The FS, BS, and T beams are used to calculate the $R(FS/BS)$ and $R(FS/T)$. An important and useful property of these two intensity ratios are their lack of dependence on the incident beam, experimental geometry, detector efficiency, and other properties of the experimental setup, since these effects are similar in the numerator and in the denominator of a ratio and, therefore, cancel out once the ratio is computed, with the exception of the path length correction as follows.

The necessary corrections for path length differences associated with varying x-ray geometry can be completed by using the following simple procedures:

1. When the FS-BS technique is used, the relative changes in the intensities for two energy regions through the equal length paths denoted by (3-4) and (4-3) for FS and BS in Fig. 2 are measured.
2. If the FS-T method is used, the change due to attenuation in the intensity of the beam of energy E_0 that passes through the (3-4) path should be measured relative to the intensity of the beam that passes through the (1-2) path, as shown in Fig. 2, which has a different length than that of the (3-4) path.

II.B. The experimental setup. Three measured intensities of the forward scattered, backscattered, and transmitted radiation were used in this study to calculate the $R(FS/BS)$ and $R(FS/T)$ ratios. In order to compensate for the differences in the penetration abilities of the FS and BS beams in this study, it was necessary to repeat measurements after rotating a test object (or source–detector system) by 180° and to obtain the $(\mathrm{R(FS/BS)})^{(0°)}$ and $[R(FS/BS)]^{(180°)}$ ratios. The same technique was used to compensate for differences in the penetrability of the FS and T components for the determination of $R(FS/T)$ and involved measurements of $R(FS/T)^{(0°)}$ and $R(FS/T)^{(180°)}$. The experimental setup was designed to provide measurements of the FS, BS, and T beams at complementary angles.

The authors designed and constructed specialized steel collimators that create shielded channels, which are referred to as beam-lines at forward angles of 10°, 15°, and 20°, at backward angles equal to 170° (= 180° − 10°), 165° (= 180° − 15°), and 160° (= 180° − 20°), and at 90° and 180°, as illustrated in Fig. 2(a). A photograph of the authors' experimental setup is given in Fig. 2(b). The beam-lines were constructed from polished blocks of hot-rolled steel. Bone phantoms and other samples were placed in 6 cm diameter holes located in the middle of the steel blocks. The collimator channels were about 20 cm long on either side of the central hole. The widths were 1, 2 and 3 mm for the 10, 15, and 20 degree channels respectively to limit the linear dimensions of the cross-sectional area. The direct (0° or 180°) channel was 2 mm in width. Spectra could be taken in three forward directions at 10°, 15°, and 20° and in the complementary three backward directions (170°, 165°, and 160°) by using different sets of collimators to formulate the beam, as described above.

X-rays were generated by a single nonstabilized 80 kV(peak) x-ray tube, the only x-ray tube available in the authors' laboratory, with a tungsten target and an adjustable current of up to 1 mA. The x-ray tube current varied between 2 and 1000 μA. Photons were collected for periods of up to 60 s, depending upon the current. To avoid possible errors that can arise as a consequence of beam intensity drift or from the use of a nonstabilized tube, measurements were repeated several times in a set of consecutive data runs. All of the results presented in Figs. 4–10 below were obtained by simple arithmetic averaging of the data over the number of runs, which partially eliminates some systematic errors that contribute to data scatter. The statistical errors in Figs. 4–10 are approximately the size of the symbols used to represent the data points in these figures.

Three different types of detectors were used. The first was a NaI crystal (3.8 cm in diameter) that transmitted data to a SPECTECH (ICS10) 512-channel multichannel analyzer (MCA) card that plugged into a port on a personal computer. The second detector was an ORTEC HPGe system with a beryllium window. The third detector consisted of a relatively small ($3 \times 3 \times 1$ mm) CdTe crystal (of volume 9.0 mm^3) and associated electronics components manufactured by AMPTEK.

A set of ten calibrated trabecular bone phantoms constructed from pieces of human trabecular bone from the calcaneous immersed in Vaseline (to simulate the intratrabecular medium) were used in the measurements made in this paper. The bone mineral concentrations of the phantoms used in this study varied from 51.8 to 347.3 $\mathrm{mg/cm}^3$. These phantoms had been constructed from human bone ash immersed in Vaseline that was subsequently packed into plastic containers. The nominal wall thicknesses of the containers were 1 mm, and their dimensions and volume were $4 \times 4 \times 8$ cm and 128 cm^3, respectively. The trabecular bone phantoms of this study were fabricated and first used in the UCLA CCSR studies of the 1980s and 1990s.[5,11] Since the authors' phantoms have a simplified rectangular geometry and a homogenous structure, the results of only one side of the phantoms were irradiated, thus $\theta = 0°$. The authors' attenuation correction involved additional layers of Plexiglas and Al of 5 and 3 mm thicknesses to mimic soft tissue and cortical bone, respectively. The authors' attenuation correction is the topic of Sec. II C given below.

III. RESULTS AND DISCUSSION

III.A. (FS-BS) ratio

Complete energy spectra from an 80 kV(peak) x-ray tube transmitted through a set of ten phantoms were recorded during the authors' measurements. Figure 3 displays the incident, forward scattered, and backscattered spectra that were collected using a 166.7 $\mathrm{mg/cm}^3$ test object. The transmitted and forward scattered spectra have similar shapes due to very similar attenuation in the authors' phantoms for both cases. The same set of phantoms was used to collect FS spectra at 10°, 15°, and 20°, as well as BS spectra at 170°, 165°, and 160°. All spectra were divided into 5 keV intervals and the properties of both the transmitted and scattered beams were analyzed for each interval. The forward scattered intensity was obtained by summing the counts in 25 channels that spanned a 5 keV energy segment. In the following figures, the lowest energy (starting point) of each interval is used as the nominal energy of that interval (for example, 40 keV implies an energy interval ranging from 40 to 45 keV). Energies were obtained from readouts of the energy from a properly calibrated MCA. In the interest of brevity, only results obtained using CdTe detectors are presented in this section.

Figure 4 contains a series of plots at various fixed energies (20, 30, 40, 50, and 60 keV) of the relative intensity of the forward scattered radiation at a scattering angle of 15° ($\theta = 15°$) as a function of the mineral concentration of the irradiated trabecular bone phantoms. It is evident from Fig. 4 that, for lower energies, the relative intensity of the forward scattered radiation decreases with increasing density. These results imply that changes (increases) in the attenuation due to increasing mineral density have a greater magnitude than changes (increases) in the scattering probability due to increasing mineral density. However, at higher energies, this trend becomes less prominent. At 60 keV, the intensity of forward scattered radiation is almost constant over the full range of mineral concentrations. At lower angles, measurements were made for $\theta = 10°$ at energies of 60 keV or higher, and the intensity of the forward scattered radiation

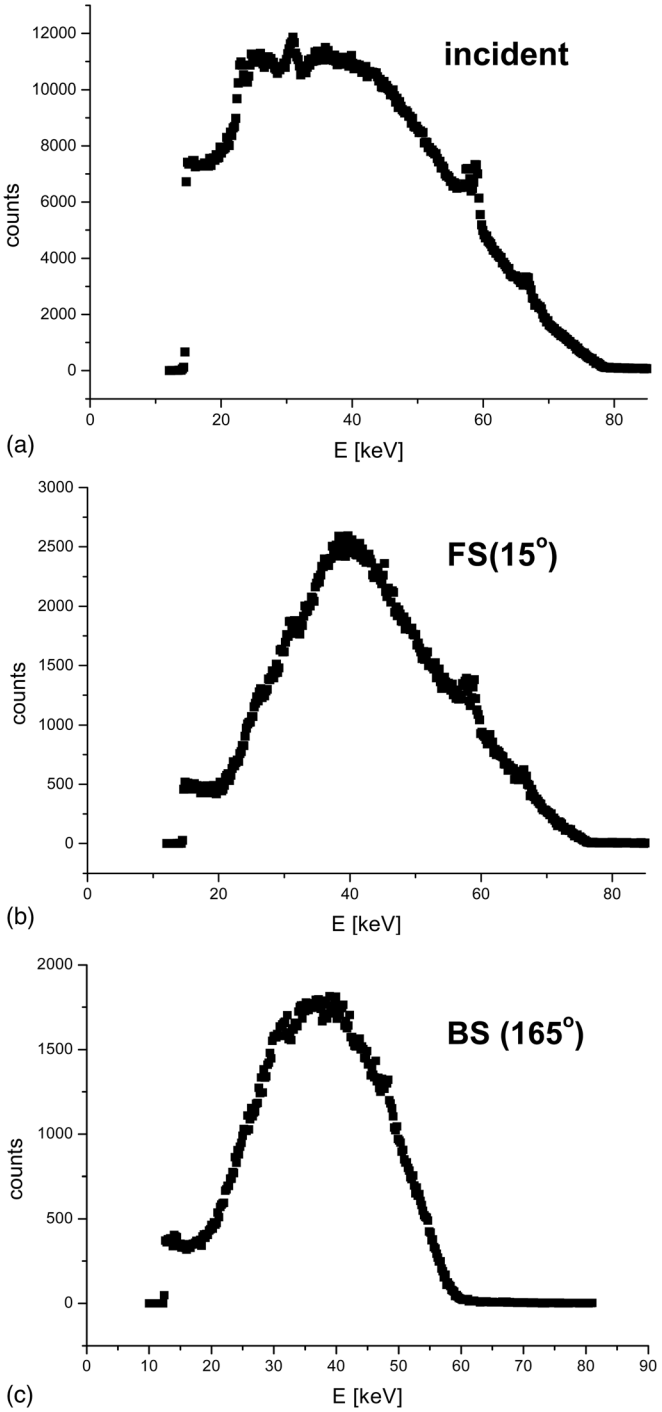

FIG. 3. Incident, forward scattered at 15°, and backscattered at 165° spectra recorded from a test object containing a mineral concentration of 166.7 mg/cm^3 using a maximum voltage of 76.5 kV are shown. The endpoint energy of the incident beam appears to be slightly higher due to the summing effect as a consequence of high count rates.

was a very slowly increasing function of mineral density. At higher energies (above 60 keV), the effects of the resulting increases in both attenuation and scattering cancel each other out by decreasing and increasing the amount of scattering in approximately equal proportions, respectively.

A high Z, material is more likely to attenuate x-ray photons of a given energy than a material with lower Z because such materials have higher scattering cross-sections, particularly for the photoelectric effect whose cross-section increases linearly with Z. In addition, the coherent scattering intensity is a strongly increasing function of atomic number. Since BMD for trabecular bone varies linearly with mean Z, one would expect that samples that have a lower TBD would attenuate radiation less readily than those with higher TBD. For the same trabecular bone sample, the coherent scattering intensity would also be expected to increase for regions with higher TBD. The shapes of the curves displayed in Fig. 4 result from a combination of the following two effects mentioned above that occur with increasing TBD: increasing amounts of photon attenuation and increasing amounts of coherent scattering.

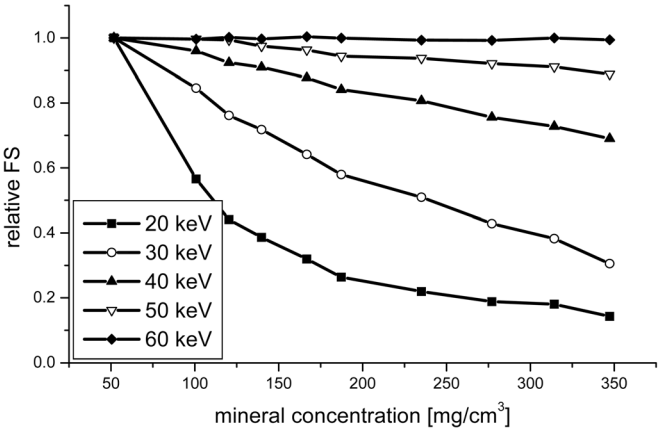

FIG. 4. The measured relative intensity of $\theta = 15°$ FS radiation as a function of the mineral density of the trabecular bone phantoms used in this study for five different fixed energies of 20, 30, 40, 50, and 60 keV.

A simple calculation based on Eq. (2) shows that the total (coherent plus Compton) intensity for photons at an incident energy of 40 keV, a scattering angle of $\theta = 15°$, a material with an atomic number of $Z = 12$, and the inclusion of the effects of attenuation along the paths of the incident and scattered beams is about 4 times lower than the corresponding scattering intensity under similar conditions in a material with $Z = 7$. However, at a higher energy of 100 keV, radiation scattered at the same angle ($\theta = 15°$) for $Z = 12$ has an intensity that is about 25% higher than that of the analogous case with $Z = 7$. In both cases, it was assumed that the densities (for $Z = 7$ and $Z = 12$) were 1×10^3 and 1.9×10^3 kg/m^3, respectively. It was also assumed that photons travel a path length of 4 cm in the material before scattering and in the material after scattering. This calculation made use of the total mass attenuation coefficients from the standard online NIST tables.[27]

The intensity of the backward scattered radiation at slightly lower energies than that of forward scattering, due to the Compton shift, was measured at the three different backscattered angles considered in this study of $\theta = 170°$, 165°, and 160°. The relative intensity of backward scattered radiation at 165° as a function of the mineral density of the scattering medium is plotted in Fig. 5. The energies tabulated in Fig. 5 (20, 30, 40, 50, and 60 keV) represent the initial energy of the beams prior to shifts due to Compton or coherent scattering. This convention implies that the 40 keV curve in Fig. 5 corresponds to a scattered photon energy interval

from 34.7 (40 keV before Compton scattering) to 38.4 keV (45 keV before Compton scattering). The relative intensity of the backscattered radiation is a uniformly decreasing function of mineral density, even for the highest energies. This uniform dependence can be explained by the simple fact that backward scattered radiation is mostly composed of Compton scattered photons, which are not as sensitive to atomic number (Z) as are coherently scattered photons. Because an increase in Z yields a moderate enhancement in the intensity of the Compton scattered radiation, but not a large enough increase to compensate for the significant loss in intensity due to the increase in attenuation. Therefore, as backward scattered photons propagate through materials, the effects of attenuation dominate and a significant and continuous decrease in the intensity of the backward scattered radiation as a function of mineral density is evident even at higher energies.

It can be seen (from Figs. 4 and 5) that the dependence of intensity on mineral density for both the FS and BS beams is very similar with one significant difference; for a single selected energy, the intensity of the FS radiation decreases more slowly than the intensity of BS radiation when mineral density is increased. From this result, one would expect that the FS-BS ratio would vary with mineral density. In Fig. 6, the FS-BS ratio is plotted for spectral segments that are 5 keV in width as a function of phantom bone mineral density for five different energies (20, 30, 40, 50, and 60 keV). The graphs in Fig. 6 contain the results of measurements that were made on a sample that was irradiated on one side only (at an incidence angle of $\theta = 0°$). In more realistic situations, the FS-BS ratio depends upon the attenuation in both the forward and backward directions. The product of two FS-BS measurements in opposite directions (at angles of 0° and 180°) is independent of possible asymmetries in the cortical bone in the forward or backward directions [as indicated by Eqs. (7) and (8)]. Since the authors' bone phantoms have a homogeneous structure and a simplified rectangular geometry that does not closely emulate the x-ray properties of *in vivo* bone, we did not perform an attenuation correction on the data presented in Fig. 6.

A close examination of Fig. 6 reveals that the 40 keV curve exhibits the strongest dependence on mineral density and, therefore, has the largest slope in a linear fit, while the slopes of the other curves are lower, thus we expect that the FS-BS ratio would have a local maximum at some intermediate energy.

III.B. FS-T ratio

In order to limit statistical errors, scattered radiation was detected using a maximum tube current of 1 mA that resulted in a transmitted x-ray beam intensity, which was too high for the authors' sensitive CdTe and NaI detectors. With the intention of reducing spectral distortion and the high dead-time that results from high intensity, the count rate was reduced by increasing the phantom-to-detector distance to values that sometimes exceeded 2 m. A second method was used to limit problems due to high intensities and high count rates that involved measurements of the spectrum of the transmitted radiation that were made separately with a low tube current of about 5 μA, without simultaneously collecting the scattered radiation. The usage of filters to limit the count rate for the transmitted radiation was not considered in order to avoid changes in the spectral shape caused by (energy-dependent) selective filtration. The relative intensity of the transmitted radiation as a function of the mineral density of the scattering medium is presented in Fig. 7 for five different energies of 20, 30, 40, 50, and 60 keV. As one might expect, the relative intensity of the transmitted radiation in this figure is a decreasing function of density.

In this study, the FS-T ratio was calculated for three forward scattering angles ($\theta = 10°$, 15°, and 20°), and it was established that FS-T is a uniformly increasing function of energy over the entire range of energies above 30 keV (up to 60 keV). In Fig. 8, the FS-T ratio for segments that are 5 keV in width is plotted as a function of phantom bone mineral density for three different energies (equal to 20, 30, and 60 keV). The slope of the curve describing the dependence of the relative FS-T ratio on mineral density is a function of energy as in the case for the FS-BS ratio plotted in Fig. 6.

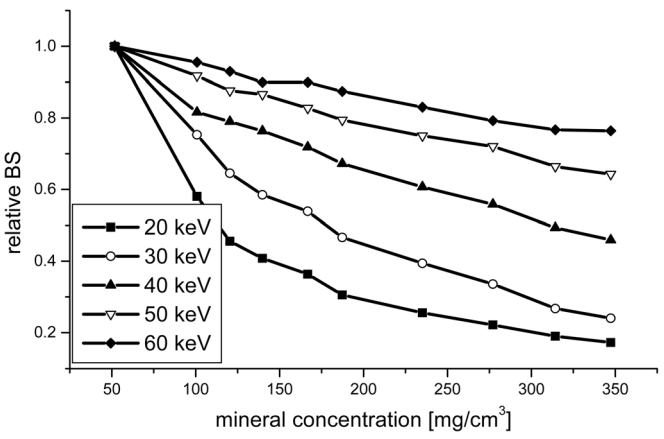

FIG. 5. The experimentally obtained relative intensity of $\theta = 165°$ backward scattered radiation as a function of the mineral density of the trabecular bone phantoms at energies of 20, 30, 40, 50, and 60 keV.

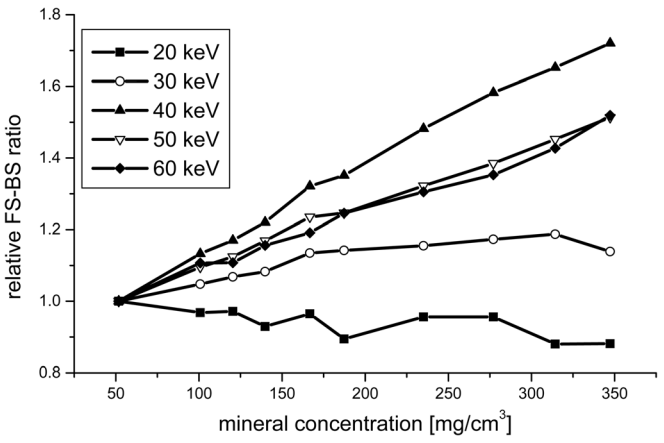

FIG. 6. The FS–BS ratio measured at a fixed forward scattering angle of $\theta = 15°$ and a backscatter angle of $\theta = 165°$ as a function of the mineral density of the trabecular bone phantoms is plotted in this figure for each of five different fixed energies (20, 30, 40, 50, and 60 keV).

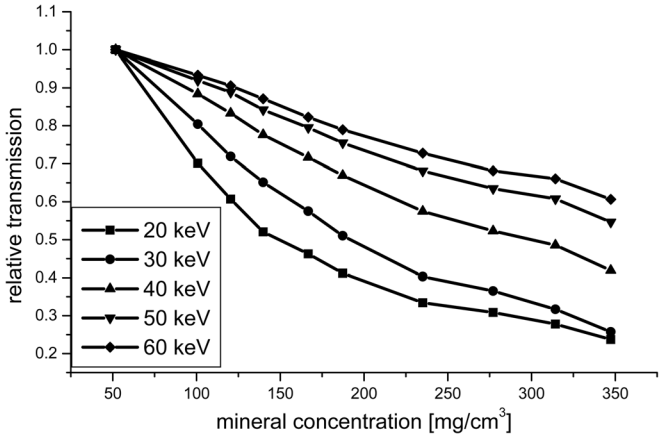

FIG. 7. The relative intensity of the transmitted radiation as a function of the mineral density of the trabecular bone phantoms is given at each of five different energies (20, 30, 40, 50, and 60 keV).

However, for very broad energy intervals, the FS-T ratio is almost a constant as a function of energy (E). For a scattering angle of $\theta = 10°$, the dependence on energy of the FS-T ratio and of the transmission (T) for phantom 1 relative to phantom 10 ([FS-T](1)/[FS-T](10)(E)) and T(1)/T(10), with phantoms 1 and 10, respectively, having the lowest and highest mineral concentrations, is plotted in Fig. 9. The FS-T plot in Fig. 9 is uniformly increasing but becomes nearly horizontal at energies of 40 keV or higher and approaches a maximum value of about 1.95 asymptotically. Very similar behavior to that of the first (FS-T) graph in Fig. 9 was observed for the other two scattering angles ($\theta = 15°$ and 20°) with a maximal value of the [FS-T](1)/[FS-T](10)(E) plot decreasing with increasing θ. For example, the maximum value of [FS-T](1)/[FS-T](10) is about 1.60 for $\theta = 15°$ and about 1.5 at $\theta = 20°$.

The mineral concentration of the trabecular bone phantoms used in this study varied from 50.8 mg/cm^3 for phantom 1 to 347.3 mg/cm^3 for phantom 10. To obtain general information on attenuation, a relative transmission index denoted by the quantity T(1)/T(10) was defined as the ratio of the intensity of radiation transmitted through the lowest concentration phantom to that of the highest concentration. The second graph in Fig. 9 displays the dependence on energy (E) of T(1)/T(10), the relative transmission index, and shows that this quantity can change quite rapidly with E. For example, Fig. 9 indicates that a standard diagnostic x-ray that produces a transmission image can yield a maximal difference in the relative transmission index between phantom 1 and phantom 10 of 64% at 60 keV. Figure 9 also shows that the transmission index between phantoms 1 and 10 can vary by as much as a factor of 4 at lower energies of about 30 keV, although such low energies are rarely used in diagnostic bone imaging due to the resulting low level of x-ray penetration. As suggested in the first curve of Fig. 9, differences in the FS-T ratio between phantom 1 and phantom 10 at 60 keV can exceed 90%. Figure 9 also shows that the value of the FS-T ratio for phantom 1 relative to phantom 10 ((FS-T)(1)/FS-T(10)) is higher than that of the transmission ratio (T(1)/T(10)) ratio in the energy region above 50 keV.

III.C. The attenuation correction

Variable attenuation coefficients and pathlengths in the paths of forward and backward scattered photons can be taken into account using the attenuation correction factor of Eq. (10). In order to accurately calculate $R_{FS/BS}$ from Eq. (7), the product of the FS-BS ratio measured from two opposite directions should be corrected for variable attenuation using $I(E_B(3\text{-}4))/I(E_0(3\text{-}4))$ as a multiplicative factor. Assuming that E_0 and E_B are the higher and lower energies, respectively, this attenuation correction factor is always less than 1 because the term $\exp(-\mu(E_0)x)$ in the numerator is always lower than the corresponding term in the denominator ($\exp(-\mu(E_B)x)$). Increases in the mineral density of the sample will decrease the attenuation correction factor due to selective attenuation. Since the radiation intensity at the

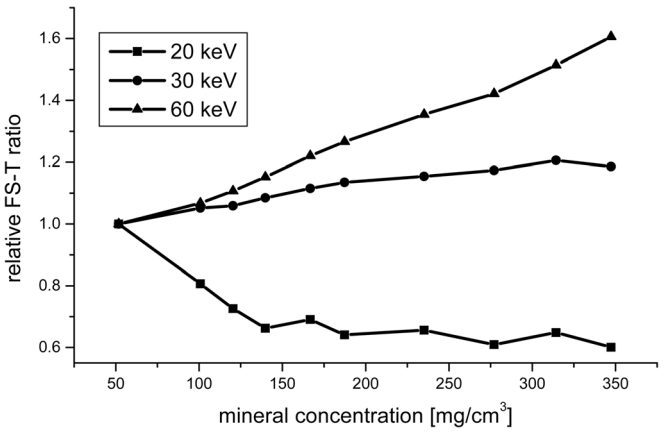

FIG. 8. The relative FS–T ratio measured at a forward scattering angle of $\theta = 15°$ as a function of the mineral density of the trabecular bone phantoms for each of three different fixed energies (20, 30, and 60 keV). Beginning at 35 keV, all relative FS–T ratios have almost an identical slope; therefore, only the 60 keV curve is given.

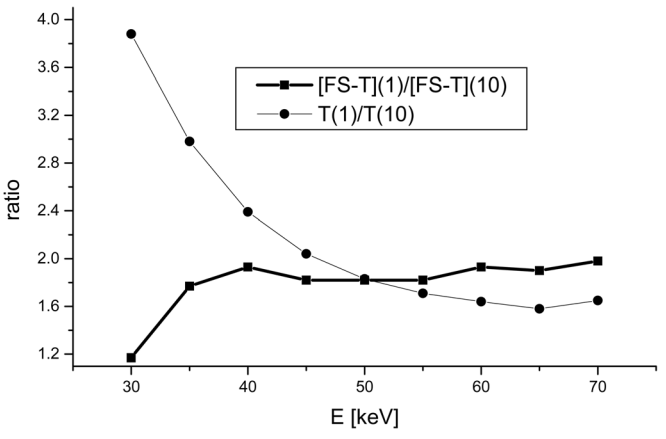

FIG. 9. The ratio of the FS–T for the trabecular bone phantom of lowest mineral concentration (phantom #1) to that of the phantom of highest mineral concentration (phantom #10) FS–T (1)/FS–T(10) as a function of x-ray energy for a scattering angle of $\theta = 10°$. This ratio is compared with a transmission index (the ratio of the intensity of radiation transmitted through phantom #1 to that of phantom #10 as a function of x-ray energy (E), T(1)/T(10)).

lower energy will decrease more quickly than the intensity at the higher energy, the factor $I_R(E_B(3\text{-}4))/I_R(E_0(3\text{-}4))$ becomes a decreasing function of mineral density. To study the decreasing trend in the correction function, the following simple calculation was performed in which the correction factor was defined to be

$$\frac{\exp\left(-\mu_{SB}(E_B)x_{SB}-\mu_{TB}(E_B)x_{TB}-\mu_{ST}(E_B)x_{ST}\right)_{3-4}}{\exp\left(-\mu_{SB}(E_0)x_{SB}-\mu_{TB}(E_0)x_{TB}-\mu_{ST}(E_0)x_{ST}\right)_{3-4}}. \quad (11)$$

In this expression, the indexes SB, TB, and ST denote solid bone, trabecular bone, and soft tissue, respectively, and the subscript 3-4 represents the integral attenuation calculated over the 3-4 path of Fig. 2(a). The authors' calculations involved the attenuation coefficients of aluminum and Plexiglas for solid bone and soft tissue. We assumed that the trabecular bone was surrounded by 3 mm of solid (cortical) bone and 5 mm of soft tissue. The thickness of the trabecular bone was chosen to be 4 cm in order to match the thickness of the phantoms. The attenuation coefficients for different values of Z, ranging from 7 to 12 were taken from the standard tables.[14] The computed (theoretical) values for the correction thickness are presented in Fig. 10(a) for four different energies equal to 30, 40, 50, and 60 keV.

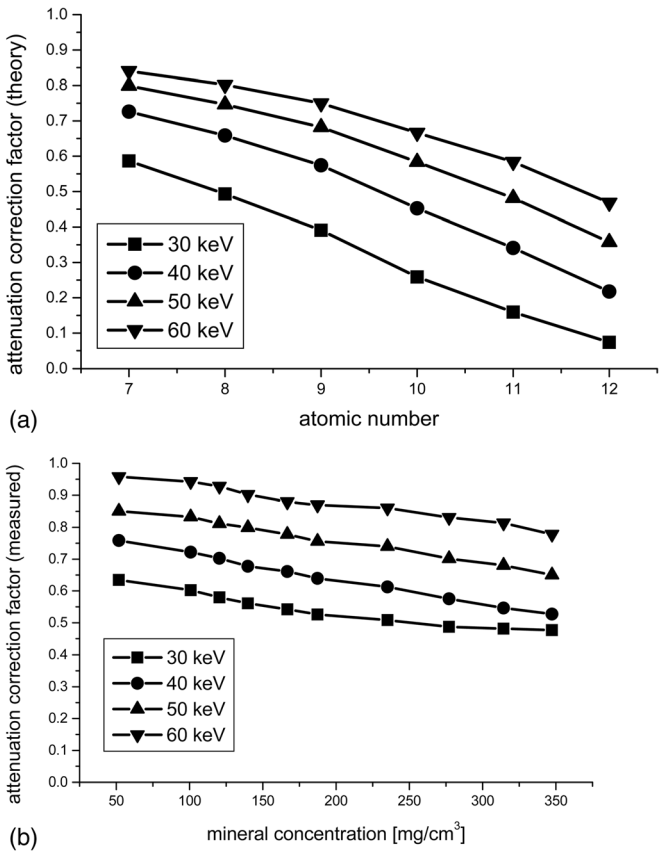

FIG. 10. (a) A simulation of the attenuation correction for the FS–BS geometry (at 15° forward and 165° backward angles) with aluminum and Plexiglas attenuators located on opposite sides of the scattering materials with mean atomic numbers ranging from $Z=7$ to $Z=12$. (b) The attenuation correction factor measured for $\theta=15°$ forward scattered and $\theta=165°$ backward scattered beams for each of four energies (30, 40, 50, and 60 keV). In order to make this correction, ten phantoms were inserted between the aluminum and Plexiglas attenuators.

To test how the multiplicative factor $I_R(E_B(3\text{-}4))/I_R(E_0(3\text{-}4))$ influences mineral density measurements in the case of nonsymmetric attenuation in an irradiated object, a 3 mm layer of aluminum was added to the scattering path on one side of a phantom and a 5 mm layer of Plexiglas was added to the scattering path on the opposite side. After measurements of the forward scattered and backward scattered radiation were completed at 0° and 180°, respectively, for each phantom, the phantoms as well as the aluminum and Plexiglas plates were removed and nonattenuated spectra were measured along the scattering path. The resulting correction factors $I_R(E_B(3\text{-}4))/I_R(E_0(3\text{-}4))$ as a function of mineral density are plotted in Fig. 10(b) for the same energies as those used in Fig. 10(a) (30, 40, 50, and 60 keV). Although realistic correction factors differ from those obtained by the authors' simplified simulation, a decreasing trend is evident in both cases. The four correction factor plots in this figure (each at fixed energy) form nearly parallel lines and the 60 keV factor changes by about 18% over the full range of mineral densities while the lower energy 40 keV factor changes by about 30% over the same range of mineral densities. The increasing trend of the FS-BS ratio as a function of energy can be compensated for through multiplication by the expression $I_R(E_B(3\text{-}4))/I_R(E_0(3\text{-}4))$, which decreases with increasing mineral density. One should bear in mind that usage of the method outlined in this section to correct for variable attenuation due to different paths can reduce the sensitivity of the FS-BS method. The accuracy of the authors' technique and the potential influence of the attenuation correction on accuracy will be determined in planned follow-up studies in the usual manner, using cadaver samples and ashed bones in order to calculate the nominal (actual) bone mineral content.

IV. CONCLUSIONS AND DISCUSSION

In this study, the original CCSR technique for determining trabecular bone mineral density, involving the use of long-lived isotopes and expensive HPGe detectors, has been significantly modified to obtain a simple and robust method for measuring quantities, which are functions of the TBD in phantoms that are usually linear in TBD. In this study, the radionuclide source has been replaced with a simple diagnostic x-ray tube and simultaneous measurements of forward scattered, backward scattered, and transmitted beams were made to calculate two possible indices of bone mineral density that may be useful in clinical settings. In particular, this study demonstrates that the FS-BS and FS-T ratios are both nearly linear functions of mineral concentration. The performance of two types of low cost detectors was also investigated to gain information on the possibility of replacing expensive and bulky HPGe detectors that must be cooled using liquid nitrogen with inexpensive counters that do not require cryogenic cooling. In this regard, we have planned future studies in which we will replace HPGe detectors by simple and inexpensive solid state detectors such as CdTe, NaI, and Si. The FS-BS and FS-T techniques described in this paper do not require high energy resolution, so NaI can be used, possibly as an integral detector, in the design of new

diagnostic devices based upon this study. Since strongly collimated beams were used in the authors' measurements and beam diameters are of the order of magnitude of a few millimeters, large detectors are not required in the methods outlined in this study. Even small CdTe detectors have a similar efficiency in the low energy region to that of large (diameter) HPGe detectors. Differences in detection efficiency between small-volume CdTe counters and large-volume HPGe and NaI detectors can be compensated for by using adequate correction functions.

The FS-BS ratio is a sensitive function of mineral density. After a correction for differences in attenuation in the forward and backward paths is undertaken, as described in this study, the FS-BS ratio becomes a function of the coherent and Compton cross-sections only. Considering the fact that, at a fixed angle (θ), both cross-sections vary solely with atomic number (Z), the FS-BS ratio can be used to make an absolute measurement of mean Z for the irradiated scattering material. One should realize that, in some cases, the correction factors for variable attenuation involving different paths can reduce the sensitivity of the FS-BS and FS-T methods outlined here. After an appropriate correction for the differences in attenuation, both the FS-BS as well as the FS-T techniques can yield a volumetric mean atomic number (BMD) for the scattering volume, in contrast to standard DXA (or DEXA), which results in an areal BMD rather than a volumetric BMD.

The most promising technique considered in this study involves usage of the FS-T ratio. At low scattering angles, FS-T can provide an index of BMD that is at least as sensitive as standard radiological methods based on the transmission of x-rays. Figure 9 demonstrates that relative FS-T over the full range of bone mineral densities considered in this paper can be up to 50% higher than a relative transmission ratio (T) at energies in the region above 60 keV. After a correction for path-dependent attenuation, FS-T can also yield a measurement of the mean atomic number of the scattering medium. The intensity of the forward scattered radiation can be an order of magnitude higher than the intensity of the backward scattered radiation, allowing for better counting statistics, shorter measurement times, and possibly lower radiation dosage to patients than that of FS-BS and traditional CCSR methods, when the FS-T technique described here is used.

The relative statistical uncertainty in the forward scattered radiation for 5 keV intervals was 2–3%, depending upon the mean energy. This error was obtained using a relatively modest maximum count rate of 50 counts/s for each 5 keV energy interval in order to limit the resulting dead time. The authors' uncertainty exposures involved duration of 60 s and a tube current of up to 1 mA. Using the methods in a standard reference,[28] we estimated that, during a single exposure, the authors' phantoms received up to 5 mSv from the authors' x-ray tube without additional filtration (with only the inherent filtration of a 1.8 mm Al slab) at a setting of 80 kV(peak). This estimate is valid only for the geometry used in the authors' *in vitro* measurements. All other possible clinical applications of the authors' technique including *in vivo* studies would require a new estimation of the dosage. Strong collimation limited the ability of the authors' setup to collect scattered radiation at extremely low solid angles of less than the order of magnitude of 10^{-4} sr. Taking into account the axial symmetry of the FS radiation, a narrow ring-shaped detector employing a significantly higher detection area can increase the collection efficiency for forward scattered radiation substantially.

If the plane of a narrow ring-shaped (annular) detector is normal to the direction of the incident beam and the center of the ring is located on the incident beam axis, only the photons scattered at the same (polar) angle (θ) and with the azimuthal angle (ϕ) within the allowed range for ϕ would be detected. It is important to realize that the angular thickness of a ring detector determines the range of angles ($\Delta\theta$), allowed by the scattering methods described in this study. From basic geometrical considerations, it can be concluded that a simple ring-shaped detector array could reduce the measurement duration, and consequently the overall dosage by up to a factor of 100. In addition, the radiation intensities obtained in the authors' measurements involved only narrow 5-keV energy intervals selected from a complete spectrum. In the FS-T technique, broad energy intervals could be used, resulting in additional significant decreases in the measurement duration and similar decreases in the dosage.

The dependence of FS-T on BMD in milligrams per cubic centimeter is presented in Fig. 8 and a relatively high potential for the diagnostic usage of the FS-T technique originates from the observation that the FS-T ratio is nearly independent of energy at energies higher than 40 keV. As can be seen from Fig. 9 presented in Sec. III, there is a broad energy region where the FS-T ratio is almost constant. The relatively weak dependence of the FS-T ratio on energy allows for the use of simple and inexpensive integral detectors instead of high resolution detectors. Thus, future FS-T diagnostic devices could avoid the need for expensive spectroscopy systems and would have relatively mild instrumentation requirements, such as the usage of a properly filtered x-ray tube and a simple integral detector for x-ray counting. The data in Fig. 9 also demonstrate that, at energies higher than 40 keV, the sensitivity of the FS-T technique is almost constant. These results imply that at a relatively strong level of filtration needs to be used in order to define an energy interval with a minimum energy at 40 keV. By using a simple and inexpensive setup consisting of a filtered x-ray tube and a ring-shaped (annular) array of detectors trabecular bone can be isolated; however, in contrast to DXA, an absolute volumetric bone mineral density rather than an areal density can be obtained as the final result. We note that the FS-T method is at least as sensitive as standard methods such as DXA based on simple transmission. If FS-T or FS-BS is applied using an appropriate experimental geometry and an annular detector array, it can effectively select only the trabecular bone and will yield a volumetric density as its final result.

The high level of precision available in DXA is the result of relatively high counting rates, which yield very good counting statistics, while accuracy is determined by errors due to the calibration and to inhomogeneities in the soft

tissue. Although the intensity of a typical beam of scattered photons is relatively low, the axial symmetry that is available in scattering experiments such as those described in this paper allows for the collection of FS radiation by an annular detector over the full range of available azimuthal angles, up to a maximum of 360°. If this ring detector also has a large area, excellent counting statistics can be obtained. The relatively small changes in the FS-T ratio, of a factor of approximately 2 for small angles of about 10°, can reach the high levels of precision only if the total uncertainty in FS-T is sufficiently low. If we make the simple assumption that the uncertainty in the authors' FS-T measurement is determined by the statistical uncertainty of the number of detected counts in the forward scattered and transmitted beams and we use the slope of the relative FS-T curve displayed in Fig. 8 to estimate an uncertainty of 1% in the intensity of the FS and T beams, we obtain an approximate error in the measured BMD of 3.7% as listed above in Table I. If the FS and T intensities were found to have a statistical uncertainty of only 0.5%, the overall error of the mineral density would be decreased to 1.5%, as given in Table I. Usage of a ring-shaped detector, with azimuthally symmetric geometry would increase the count rate by up to 2 orders of magnitude and would involve an increase the broadness of the energy interval by up to a factor of 10, resulting in an increase in the integral number of detected photons by a factor of approximately 10^4, which would reduce the statistical uncertainty by a factor of 100 (the square root of 10^4), as in Table I.

We note that, if a thick ring at a perpendicular distance r from an x-ray point source is used, the acceptance angle of the Compton scattered radiation will remain constant to first order. This effect is due to the cancellation of r^2 factors related to the increase in the ring area and the $1/r^2$ fall-off of the intensity of a point source as long as r is large compared to the mean ring radius. A ring detector can introduce significant errors due to differences in the photon paths for the various ring elements. Therefore, an estimate of the accuracy of the authors' method will have to wait until follow-up studies are completed, in which the effects of different photon paths will be determined. However, the effects of different photon paths can be minimized by a careful choice of the irradiated region to have a simple geometry that is devoid of sharp changes in the thicknesses of the cortical bone and soft tissue components. Further studies on more realistic phantoms should be performed in the near future to estimate the amount of uncertainty introduced into the final results including BMD obtained using a ring detector.

An advantage of the FS-T ratio, over other assessment techniques such as DXA and QCT, is its lack of dependence on energy over a large range of the incident energies. This energy independence property leads to several advantages, such as the possible usage of simple integral detectors, as mentioned in Sec. IV. In addition, FS-T applied using a filtered x-ray tube and the integrated count rate from an annular detector would involve a relatively inexpensive and compact system that would provide information on a selected volume inside the body, as is available with QCT. Thus, the authors' approach to FS-T would result in a system that could provide similar information to that of QCT in a clinical environment with the distinct advantages of being more accurate, less expensive, and more compact.

In follow-up studies to this paper, the sensitivity of the FS-T technique should be tested at energies higher than 80 keV to establish an optimal kilovolt peak and an optimal energy interval. Only small samples that mimic the geometry of trabecular bone would be needed for initial studies of optimal kilovolt peak and spectral intervals. In some clinical situations, the volume of the irradiated object (or region of the body) would have a significantly larger diameter, and in this case, the increase in attenuation could be compensated for by a corresponding increase in tube current, after the optimal energy range had been determined. Additional tissue would increase the overall attenuation of the incident, transmitted, and scattered beams. A general method for performing an attenuation correction is described in Secs. II A 1 c and II C. The use of samples with different diameters and geometries other than those considered in this paper should also be the subject of follow-up studies. Multiple scattering effects were not considered in this paper because the authors' experimental configuration involved relatively strong collimation. At the very least, this study will provide a significant contribution to the development bone assessment by providing additional photons, beyond those which are currently available through absorptiometry or transmission as in DXA and QCT, including coherently scattered x-rays that are highly sensitive to BMD. The extra photons also have the advantage of being obtained without increasing the dosage beyond that of standard absorptiometry or transmission methods for the chosen exposure duration since photons scattered at a known scattering angle are not currently being collected by such methods (including DXA and QCT).

ACKNOWLEDGMENTS

The authors would like to dedicate this paper to Professor Moses A. Greenfield of UCLA whose previous work and guidance inspired them to undertake the research described in this paper. They also wish to express their gratitude to the National Institutes of Health who supported this research through Grant Nos. GM 08156-22 and 1R43 AR053766-1. They greatly appreciate the expert assistance provided by Professor Shailendra Shukla of the University of Florida Gainesville and the Gainesville VA Center in the research described in this manuscript. The efforts of Amaro Moreno Jr., a BS in Physics recipient from CSUDH in May 2009, in carefully setting up and taking the photograph of the experimental setup that comprises Fig. 2(b), are also greatly appreciated.

[a]Electronic mail: kganezer@csudh.edu

[1]P. Puumalainen, A. Uimarihuhta, E. Alhava, and H. Olkkonen, "A new photon scattering method for bone mineral density measurements," Radiology **120**, 723–724 (1976).
[2]J. T. Stalp and R. B. Mazess, "Determination of bone density by coherent-Compton scattering," Med. Phys. **7**, 723–726 (1980).
[3]A. Karellas, I. Leichter, J. D. Craven, and M. A. Greenfield, "Characterization of tissue via the coherent-to-Compton scattering ratio," Med. Phys. **10**, 605–609 (1983).

[4]I. Leichter, A. Karellas, J. D. Craven, and M. A. Greenfield, "The effect of the momentum transfer on the sensitivity of a photon scattering method for the characterization of tissues," Med. Phys. **11**, 31–36 (1984).
[5]I. Leichter, A. Karellas, S. S. Shukla, J. L. Looper, J. D. Craven, and M. A. Greenfield, "Quantitative assessment of bone mineral by photon scattering: calibration considerations," Med. Phys. **12**(4), 466–468 (1985).
[6]S. A. Kerr, K. Kouris, C. E. Weber, and T. J. Kennett, "Coherent scattering and the assessment of mineral concentration in trabecular bone," Phys. Med. Biol. **25**, 1043–1047 (1980).
[7]E. Odebland and Å. Norhagen, "Measurement of electron densities with the aid of the Compton scattering process," Acta Radiol. **45**, 161–168 (1955).
[8]G. E. Gigante and S. Sciuti, "A large-angle coherent/Compton scattering method for measurement in vitro of trabecular bone mineral concentration," Med. Phys. **12**(3), 321–326 (1985).
[9]G. D. Guttman and M. M. Goodsitt, "The effect of fat on the coherent-to-Compton scattering ratio in the calcaneous: A computational analysis," Med. Phys. **22**(8), 1229–1234 (1995).
[10]A. M. Ndlovu, T. J. Farrell, and C. E. Webber, "Coherent scattering and bone mineral measurement: The dependence of sensitivity on angle and energy," Med. Phys. **18**, 985–989 (1991).
[11]S.-S. Ling, S. Rustigi, A Karellas, J. D. Craven, J. S. Whiting, M. A. Greenfield, and R. Stern, "The measurement of trabecular bone mineral density using coherent and Compton scattered photons in vitro," Med. Phys. **9**, 208–215 (1982).
[12]S. S. Shukla, A. Karellas, I. Leichter, J. D. Craven, and M. A. Greenfield, "Quantitative assessment of bone mineral by photon scattering: Accuracy and precision consideration," Med. Phys. **12**(4), 447–448 (1985).
[13]S. S. Shukla, I. Leichter, A. Karellas, J. D. Craven, and M. A. Greenfield, "Trabecular bone mineral density measurement in-vivo: Use of the ratio of coherent to Compton scattered photons in the calcaneous," Radiology **158**, 695–697 (1986).
[14]M. A. Greenfield, J. D. Craven, and S. S. Shukla, "Bone mineral measurements using the method of coherent to Compton scattered photons in the calcaneous," in *In Vivo Body Composition Studies*, edited by K. J. Ellis *et al*. [The Institute of Physical Sciences in Medicine (IPSM), London, 1989], Chap. 14.
[15]T. N. Hangartner and D. F. Short, "Accurate quantification of width and density of bone structures by computed tomography," Med. Phys. **37**, 3777–3784 (2007).
[16]S. R. Cummings, D. Bates, and Dennis M. Black, "Clinical use of bone densitometry: Scientific review," J. Am. Med. Assoc. **288**(15), 1889–1897 (2002).
[17]H. K. Genant *et al*., "Noninvasive assessment of bone mineral and structure: State of the art," J. Bone Miner. Res. **11**(6), 707–730 (1996).
[18]M. A. Greenfield, "Current status of physical measurements of the skeleton," Med. Phys. **19**(6), 1349–1357 (1992).
[19]P. Tothill, "Methods of bone mineral measurement," Phys. Med. Biol. **34**, 543–572 (1989).
[20]M. Krmar, S. Shukla, and K. Ganezer "Bone densitometry using x-ray spectra," Phys. Med. Biol. **55**(20), 6105–6123 (2010).
[21]P. M. Joseph, and C. Ruth, "A method for simultaneous correction of spectrum hardening artifacts in CT images containing both bone and iodine," Med. Phys. **24**, 1629–1634 (1997).
[22]M. A. Greenfield, J. D. Craven, A. Huddleston, M. L. Kehrer, D. Wishko, and R. Stern, "Measurement of the velocity of ultrasound in human cortical bone in vivo," Radiology **138**, 701–710 (1981).
[23]K. Krishna Murthy *et al*., "Verification of setup errors in external beam radiation therapy using electronic portal imaging," J. Med. Phys. **33**(2), 49–53 (2008).
[24]M. M. Goodsitt, "Beam hardening errors in post-processing dual energy quantitative computed tomography," Med. Phys. **22**, 1039–1047 (1995).
[25]M. Krmar, K. Ganezer, and S. Shukla, "A new radiological method for the determination of trabecular bone mineral density (TBMD) in-vivo," Abstract Submitted to the American Association of Physicists in Medicine (AAPM) 45th Annual Meeting, August 2003, San Diego, CA, Poster Presentation PO-I-21, Med. Phys. **30**(6), 1463 (2003).
[26]J. H. Hubbell, W. J. Veigele, E. A. Briggs, P. T. Brown, D. T. Cromer, and R. J. Howerton, "Atomic form factors, incoherent scattering functions, and photon scattering cross-sections," J. Phys. Chem. Ref. Data **4**, 471–538 (1975).
[27]M. J. Berger, J. H. Hubbell, S. M. Seltzer, J. Chang, J. S. Coursey, R. Sukumar, and D. S. Zucker, "XCOM: Photon cross-sections database," http://physics.nist.gov/PhysRefData/Xcom/Text/XCOM.html.
[28]J. Shapiro, *Radiation Protection: A Guide for Scientists, Regulators, and Physicians*, 4th ed. (Harvard University, Cambridge, 2002).